ACCSCIENCE PUBLISHING

International Journal of Bioprinting

RESEARCH ARTICLE

3D-bioprinted osteocytes expressing Wnt7b protect osteoblast differentiation from microgravity

Jinling Zhang[1†], Pengtao Wang[1†], Xiaoling Chen[1], Saima Khan[1], Haiping Ouyang[2], Yangxi Liu[2], Bo He[2], Xian Li[3], Xing Liu[2*], and Xiaolin Tu[1*]

[1]Laboratory of Skeletal Development and Regeneration, Key Laboratory of Clinical Laboratory Diagnostics (Ministry of Education), College of Laboratory Medicine, Chongqing Medical University, Chongqing, China

[2]Department of Orthopedics, Ministry of Education Key Laboratory of Child Development and Disorders, National Clinical Research Center for Child Health and Disorders, Children's Hospital of Chongqing Medical University, Chongqing, China

[3]College of Medical Informatics, Chongqing Medical University, Chongqing, China

Abstract

Maintaining bone formation in microgravity/weightless environments remains a major challenge. Under weightless conditions, osteocytes act as mechanosensors to inhibit Wnt canonical signaling and bone formation by secreting sclerostin. This study explores whether osteocytic Wnt7b can counteract microgravity-induced bone loss through Wnt non-canonical signaling. Unlike previous bioprinting studies that focused on structural scaffolds or generic cell types, a novel bioprinted scaffold consisting of polycaprolactone (supportive) and osteocyte (functional) hydrogels was constructed in this study. Osteocytes overexpressing Wnt7b were co-cultured with bone marrow stromal cells (ST2) in a 3D biomimetic weightless biomicroenvironmental system (3D-BWBM) to assess osteogenic and lipogenic differentiation. The results indicated that osteocytic Wnt7b enhanced osteogenic differentiation and mineralization of ST2 cells via the Wnt non-canonical pathway PKCδ, while suppressing the expression of lipogenic markers (*Pparg*, *Cebpa*) and adipogenesis. Reverse transcription quantitative polymerase chain reaction (RT-qPCR) analysis revealed elevated expression of *Sost* and *Mef2c*, downregulation of the Wnt target gene *Opg*, and elevated expression of pro-osteoclastogenic cytokine *Rankl* and pro-inflammatory cytokines *Tnfa* and *Il1b*, thus validating the microgravity effect. Unlike conventional 2D culture of RCCS™ cells, the 3D hydrogels were printed with tunnels (500 μm) for efficient nutrient/metabolite exchange, resulting in good cell growth, high cell viability (97%), and a six-fold increase in proliferative activity within 7 days. Wnt7b osteocytes were still able to maintain the osteogenic differentiation of ST2 cells, as evidenced by elevated alkaline phosphatase activity, mineralization (1.8-fold increase), and a decrease in osteoblast marker genes (*Alpl, Runx2, Col1a1*). In conclusion, Wnt7b-PCKδ signaling counteracts microgravity-induced bone loss, and further *in vivo* studies on osteocytic Wnt7b are warranted to confirm this causal relationship.

Keywords: 3D bioprinting; Microgravity; Osteogenic differentiation; Wnt7b; Wnt noncanonical signaling

[†]These authors contributed equally to this work.

***Corresponding authors:**
Xiaolin Tu
(xtu@cqmu.edu.cn)

Xing Liu
(400269@hospital.cqmu.edu.cn)

Citation: Zhang J, Wang P, Chen X, *et al.* 3D-bioprinted osteocytes expressing Wnt7b protect osteoblast differentiation from microgravity. *Int J Bioprint.* 2025;11(4):426-445. doi: 10.36922/IJB025240238

Received: June 12, 2025
Accepted: July 3, 2025
Published Online: July 3, 2025

Copyright: © 2025 Author(s). This is an Open Access article distributed under the terms of the Creative Commons Attribution License, permitting distribution and reproduction in any medium, provided the original work is properly cited.

Publisher's Note: AccScience Publishing remains neutral with regard to jurisdictional claims in published maps and institutional affiliations.

1. Introduction

Bone loss in microgravity remains a significant challenge for astronauts, with bone mineral density (BMD) of the lumbar spine and hip joint decreasing by 1–1.5% per month,[1–3] mainly due to suppressed osteoblast activity and increased osteoclast-based osteolysis.[4,5] Current countermeasures, including physical exercise, nutritional supplementation, and pharmacological protection, have limited effectiveness, potential risks, and side effects.[6] A promising alternative is to target osteocytes, the mechanosensory cells in the skeleton that regulate osteoblast/osteoclast activity through Wnt signaling.[7,8] However, the loss of mechanical loads, such as prolonged bed rest, paralysis, or space flight,[9] upregulates osteocyte sclerostin (gene: *Sost*), which blocks the binding of Wnt ligand to its coreceptor Lrp5/6. This, in turn, inhibits the Wnt/β-catenin canonical signaling pathway,[10] leading to a decrease in osteoblast differentiation.[11,12]

Wnt7b, a ligand that activates the non-canonical Wnt pathway, has emerged as a potential solution. In contrast to Wnt/β-catenin signaling, Wnt7b-PKCδ is sclerostin independent and promotes osteogenesis in mice.[13,14] We recently observed that mice with osteocyte-specific Wnt/β-catenin activation (daβcat^{Ot}) exhibit elevated Wnt7b expression (Figure 1A) and are protected from weightlessness-induced bone loss. This led us to hypothesize that osteocytic Wnt7b creates a microenvironment conducive to osteogenesis even under microgravity conditions.

The cost of conducting research under actual microgravity conditions is high, resulting in limited research opportunities. Various types of bone tissue engineering (BTE) scaffolds are widely used in microgravity environments.[15] Although scaffolds may provide temporary physical support for cell attachment, proliferation, and differentiation, the microgravity environment confers a unique mechanical environment with profound effects on cell fate.[16] Therefore, cell culture in microgravity environments could inspire greater potential for scaffold-based BTE. The use of biomaterials combined with a simulated weightlessness device for *in vitro* 3D culture provides a platform that closely mimics *in vivo* conditions, thereby supporting tissue and cell regeneration.[17,18]

Recent advances in 3D bioprinting have enabled the fabrication of bone-mimicking scaffolds with customized mechanical and biochemical properties.[19] However, most studies have focused on structural optimization (e.g., porosity, stiffness) or general effector cell (e.g., mesenchymal stem cells, osteoblasts) encapsulation, without utilizing mechanosensitive cell sources as functionalized agents to actively counteract microgravity-induced bone loss. Recent research has developed microgravity-compatible bioprinted constructs but relied on passive scaffold designs that lacked innate osteoinductive signaling.[20]

Herein, we present two key innovations: (i) bioprinting of functionalized osteocytes and (ii) a 3D biomimetic weightless biomicroenvironment (3D-BWBM) as a bionic microgravity platform. We designed Wnt7b-expressing osteocytes (MLO-Y4) as a bioactive cell source to bypass sclerostin-mediated Wnt inhibition. Unlike previous studies using undifferentiated cells, Wnt7b-activated osteocytes promoted osteogenic differentiation of undifferentiated cells via the non-canonical Wnt-PKCδ pathway while inhibiting adipogenic differentiation—a dual mechanism that is not possible with conventional scaffolds or growth factors. Likewise, by combining a 3D bioprinted polycaprolactone (PCL)-gelatin methacryloyl (GelMA) scaffold with NASA's rotating cell culture system (RCCS™), we have created 3D-BWBM that goes beyond traditional 2D RCCS™ cultures. Our system features multi-scale tunnels (500 μm) for enhanced nutrient/metabolite transport. Intercellular crosstalk is maintained by printing osteocyte-ST2 co-cultures for long-term osteogenic function under simulated microgravity conditions.

This study combines, for the first time, mechanosensitive cell customization with a 3D-bioprinted exoskeleton for microgravity applications, providing a scalable solution for disuse osteoporosis. By expanding the scope of bioprinting to realize biological functions in extreme environments, this study establishes a critical link between biomanufacturing and space medicine.

2. Materials and methods

2.1. Materials

Puromycin (10 mg/mL stock solution), Rottlerin (PKCδ inhibitor, dissolved in dimethyl sulfoxide [DMSO], stored at 10 mM), rapamycin (mTORC inhibitor, dissolved in DMSO, stored at 50 mM), and iCRT-14 (Wnt canonical signaling inhibitor, dissolved in DMSO, stored at 50 mM) were purchased from MedChemExpress (China). The BCIP/NBT Alkaline Phosphatase Color Development kit, modified Oil Red O staining kit, calcein/PI cell viability/cytotoxicity assay kit, alkaline phosphatase (AP) assay kit, phenylmethanesulfonyl fluoride (PMSF), RIPA lysis buffer, the nuclear and cytoplasmic protein extraction kit, phosphatase inhibitors, and DAPI staining solutions were obtained from Beyotime Biotechnology (China). TRizol reagent, Evo M-MLV reverse transcription premix kit, and SYBR Green Premix Pro Taq HS qPCR kit were obtained

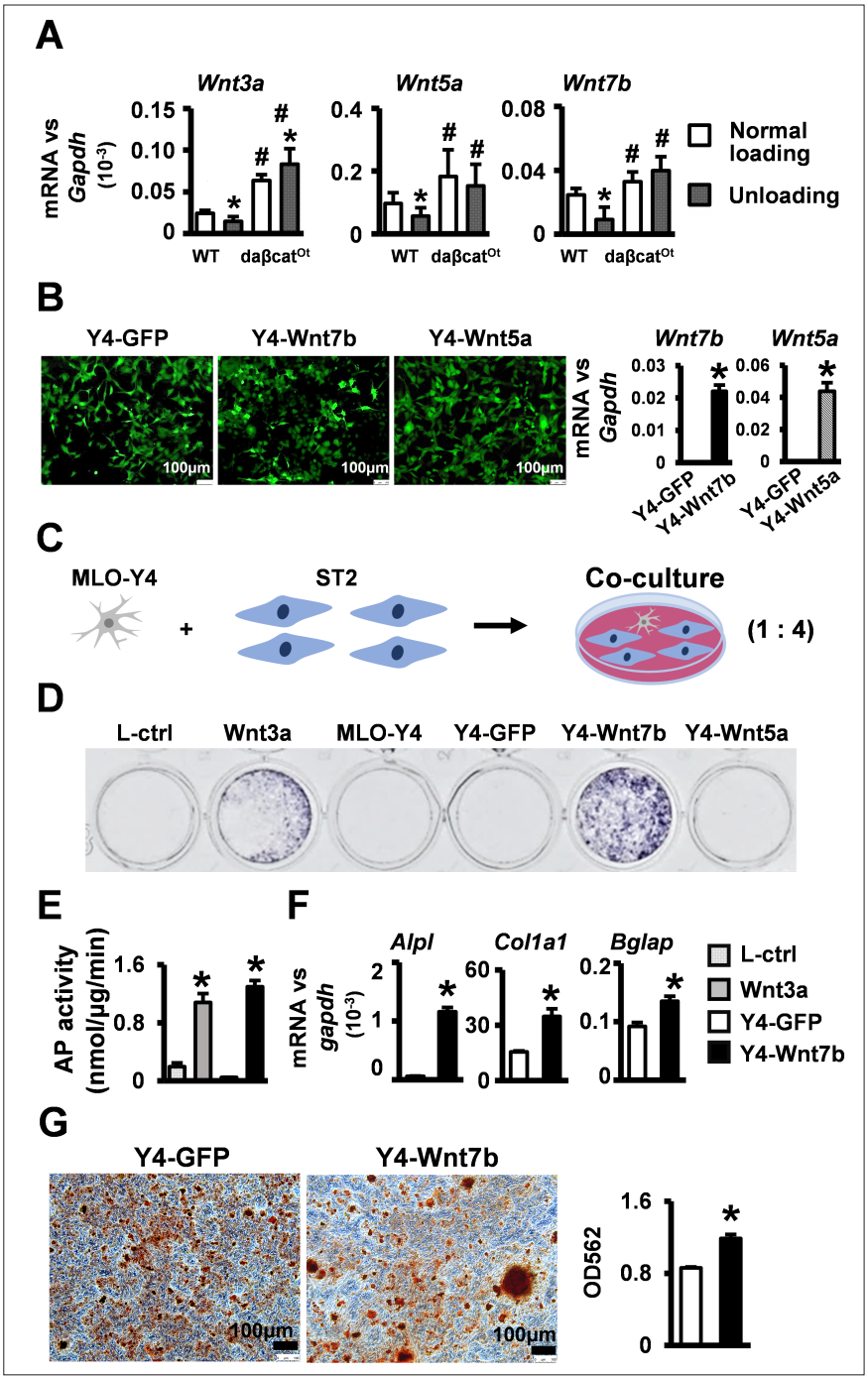

Figure 1. Effect of osteocytic Wnt7b on the osteogenic differentiation of ST2 cells. (A) Expression levels of Wnt ligands (Wnt3a, Wnt5a, Wnt7b) in the tibia and femur of 16-week-old daβcat^{Ot} mice and WT controls after 14 days of tail suspension, measured by RT-qPCR. Data are presented as mean ± standard deviation; *$p < 0.05$ versus normal loading; #$p < 0.05$ versus WT, by Two-Way ANOVA, $n = 5–7$. (B) Images and gene expression of the osteocytic cell line MLO-Y4 cells infected by lentiviruses expressing Wnt7b, Wnt5a, and their control GFP, respectively. Scale bar = 100 μm. (C) Schematic of the co-culture model: MLO-Y4 osteocytes and ST2 bone marrow stromal cells were co-cultured at a 1:4 ratio. (D) AP staining after 3 days of co-culture. L-ctrl and Wnt3a groups represent MLO-Y4 cells treated with control or Wnt3a-conditioned medium, respectively. MLO-Y4, Y4-GFP, Y4-Wnt7b, and Y4-Wnt5a represent co-culture of ST2 cells with the corresponding MLO-Y4 osteocytes. (E) AP biochemical activity assay of the co-culture as indicated. (F) Expression of osteoblast marker genes (*Alpl*, *Col1a1*, *Ibsp*, *Bglap*) of the co-culture as indicated. (G) Alizarin Red S staining and quantification of mineralization nodules of the co-culture of Y4-GFP and Y4-Wnt7b. Scale bar: 100 μm. *$p < 0.05$, compared with Y4-GFP or L-ctrl by Student's *t*-test, $n = 3$ for panels B, E, F, and G. Abbreviations: AP, alkaline phosphatase; daβcat^{Ot}, mice with daminantly active Wnt/β-catenin in osteocytes; GFP, green fluorescent protein; mRNA, messenger ribonucleic acid; RT-qPCR, reverse transcription quantitative polymerase chain reaction; WT, wide type.

from Accurate Biotechnology (China). Lyophilized GelMA and photo-crosslinking agent lithium phenyl-2,4,6-trimethylbenzoylphosphinate (LAP) were obtained from Sunp Biotech (China). Hydrocortisone, 3-isobutyl-1-methylxanthine (IBMX), indomethacin, PCL, and polybrene were obtained from Sigma (United States of America [USA]). The quantitative polymerase chain reaction (qPCR) primers were synthesized by Sangon Biotech (China). Alizarin Red S (ARS), β-glycerophosphate disodium salt solution, and L-ascorbic acid were obtained from Solarbao Biotechnology (China). The Cell Counting Kit-8 (CCK-8) was obtained from Yeasen Biotechnology (China). Phosphate-buffered saline (PBS) and SDS-PAGE gels were obtained from Epizyme Biotech (China).

Rabbit polyclonal anti-mouse β-catenin antibody, Lamin B1 polyclonal antibody, MARCKS polyclonal antibody, and phospho-MARCKS (Ser159/163) polyclonal antibody were purchased from Proteintech (China). Cy3-labeled goat anti-rabbit IgG (H+L) was obtained from Beyotime Biotechnology (China). Polyclonal anti-Gapdh antibody and secondary antibody goat anti-rabbit IgG H&L (HRP) were obtained from ZENBIO (China).

Alpha modified eagle's minimum essential medium (α-MEM) and Dulbecco's modified eagle (DMEM) medium were purchased from Gibco (USA). The penicillin-streptomycin solution (100×) was obtained from Beyotime Biotechnology (China). Fetal bovine serum (FBS) was obtained from Biological Industries (Israel).

2.2. Cell lines and cell culture

The osteocytic cell line (MLO-Y4) was provided by Professor Lynda Bonewald, Indiana University School of Medicine, and the ST2 cells were provided by Dr. Steve Teitelbaum, Washington University. Both cell lines were cultured in α-MEM growth medium supplemented with 10% FBS and 1% penicillin-streptomycin. Wnt3a-expressing cells (Wnt3a) and their control cells (L-ctrl) were purchased from the American Type Culture Collection (ATCC, USA) and cultured in DMEM growth medium containing 10% FBS and 1% penicillin-streptomycin. All cells were cultured in an incubator with 5% CO_2 at 37°C.

MLO-Y4 cells stably transfected with lentivirus expressing green fluorescent protein (GFP) (control), Wnt7b, and Wnt5a were labeled as Y4-GFP, Y4-Wnt7b, and Y4-Wnt5a, respectively. For co-culture experiments, Y4 (1×10^4 cells/well) and ST2 cells (4×10^4 cells/well) were seeded together in 24-well plates and cultured for 3 days or as otherwise indicated. Osteogenic differentiation was assessed by AP staining after co-culturing MLO-Y4 and ST2 at 1:2, 1:4, 1:6, and 1:8 ratios, respectively.

2.3. Isolation of long bones of tail-suspended mice for RNA extraction

Mice with dominantly active β-catenin in osteocytes (daβcat^{Ot}) and wild-type control mice (WT) were generated as previously reported.[21] Briefly, DMP1-8kb-Cre mice expressing Cre recombinase in osteocytes were crossed with Catnb$^{lox(ex3)/lox(ex3)}$ mice, in which exon 3 of the β-catenin gene (encoding the degradation domain) is flanked by LoxP sites. All animal procedures were approved by the Institutional Animal Care and Use Committee of Chongqing Medical University and conducted in accordance with relevant guidelines (IACUC-CQMU-2024-0277).

The 14-week-old daβcat^{Ot} and WT mice underwent suspension for 14 days.[22] Following euthanasia, tibiae and femurs were dissected, and soft tissue (skin, muscle) was meticulously removed. After clipping the femoral epiphysis, the bone marrow was flushed three times with α-MEM containing 1% FBS. The cleaned long bone shafts were immediately snap-frozen in liquid nitrogen and stored in –80°C until RNA extraction.

2.4. Stable transfection of MLO-Y4 with lentivirus

MLO-Y4 cells overexpressing Wnt7b or Wnt5a were generated via stable lentiviral transduction, as previously described.[23] Lentiviruses expressing Wnt7b, Wnt5a, and GFP were purchased from GENECHEM (China). MLO-Y4 cells were transfected at a multiplicity of infection (MOI) of 100 in the presence of 7 μg/mL polybrene. Transfection efficiency was assessed 48 h post-infection by GFP fluorescence intensity. Transfected cells were selected and maintained in culture medium containing 0.5 μg/mL puromycin for at least 1 week to eliminate non-transfected cells.

2.5. RNA extraction and quantitative real-time PCR

Total RNA was extracted from long bone shafts or cultured cells using TRIzol reagent according to the manufacturer's instructions, as previously described.[23] Complementary DNA (cDNA) was synthesized using the Evo M-MLV reverse transcription premix kit, and qPCR was performed using the SYBR Green Premix Pro Taq HS qPCR kit in the CFX Connect Real-Time PCR Detection System (Bio-Rad Laboratories, USA). All primer sequences are listed in Table 1. All qPCR reactions were performed three times. The relative mRNA expression levels were calculated using the $2^{-\triangle CT}$ method, with the housekeeping gene glyceraldehyde-3-phosphate dehydrogenase (*Gapdh*) as the reference gene.

2.6. Alkaline phosphatase staining

Alkaline phosphatase (AP) staining was performed as described previously.[23] Cells were washed with 1× PBS and fixed with 3.7% formaldehyde (Chongqing Chuandong Chemical Group, China) for 5 min at room temperature. Fixed cells were then incubated with staining solution from the BCIP/NBT Alkaline Phosphatase Color Development Kit according to the manufacturer's protocol for 30 min at room temperature. For the PCL and cell-integrated 3D-printed (PCI3D) modules, staining was performed after 7 and 14 days of culture, with the staining duration extended to ≥4 h. Stained samples were imaged using a standard digital camera.

2.7. Alkaline phosphatase biochemical activity assay

The AP biochemical activity assay was quantified as previously described.[23] Briefly, cells were washed with PBS and lysed in 300 μL of 10 mM Tris/HCl (pH 7.4) per well. Lysates were scraped, sonicated on ice, and centrifuged at 13,000 rpm for 3 min at 4°C. The supernatant was collected, and AP activity was measured using the AP assay kit following the manufacturer's instructions. Absorbance at 405 nm was recorded using a VarioskanTM LUX multimode microplate reader (Thermo Fisher Scientific, USA).

2.8. Mineralization assay

Mineralized matrix deposition was assessed by ARS staining, as previously described.[23] Osteocytes and ST2 cells were seeded in 24-well plates or PCI3D modules and cultured in growth medium for 3 or 7 days, respectively. Osteogenic differentiation was then induced by culturing the cells for 14 days in osteogenic medium consisting of growth medium supplemented with 10 mM β-glycerophosphate disodium and 50 μg/mL L-ascorbic acid. Cells or modules were fixed with 3.7% formaldehyde for 3 min and stained with 0.4% ARS solution (pH 4.2) for 30 min. Stained samples were imaged under a microscope. To quantify mineralization, the ARS stain was eluted with 10% cetylpyridinium chloride (CPC) for 1 h. The eluent was collected, and absorbance was measured at 562 nm to quantify the mineralization status.

2.9. Western blotting

Western blotting was conducted following standard procedures.[24] Total proteins were extracted by lysing cells in RIPA lysis buffer containing PMSF and phosphatase inhibitors. Cytoplasmic and nuclear protein fractions were isolated using a nuclear and cytoplasmic protein extraction kit. Protein samples (20 μg per lane) were separated by 10% SDS-PAGE and transferred onto 0.22 μm polyvinylidene fluoride (PVDF) membranes (Boster

Table 1. Sequences of primers used for qPCR

Gene	Primer sequence (5'–3')	
	Forward	Reverse
Gapdh	GCACAGTCAAGGCCGAGAAT	GCCTTCTCCATGGTGGTGAA
Wnt3a	CTTAGTGCTCTGCAGCCTGA	GAGTGCTCAGAGAGGAGTACTGG
Wnt5a	TTGGCCACGTTTTTCTCC	TGGCTGCAGAGAGGCTGT
Wnt7b	GCCTCATGAACCTTCACAAC	AACTTAGGTAGCGTGGTCCA
Alpl	TTCGCTATCTGCCTTGCCTG	AGTCTGTGTCTTGCCTGCC
Runx2	CCGTGGCCTTCAAGGTTGT	TTCATAACAGCGGAGGCA
Col1a1	TCAACCCCGTCTACTTCCCT	TTCAACAGTCCAAGAACCCCAT
Bglap	GCCTACAAACGCATCTACGG	GAGAGAGAGGACAGGGAGGA
Sp7	GCCCCCTGGTGTTCTTCATT	CTTCCCCCTTCTTGGCACTC
Ibsp	CAGAGGAGGCAAGCGTCACT	GCTGTCTGGGTGCCAACACT
Axin2	TGAGCGGCAGAGCAAGTCCAA	GGCAGACTCCAATGGGTAGCT
Pparg	AGCCCTTTACCACAGTTGATTTCTCC	GCAGGTTCTACTTTGATCGCACTTTG
Cebpa	TGGACAAGAACAGCAACGAG	TCACTGGTCAACTCCAGCAC
Mef2c	AAGCCTCAGCATCAAGTCAGAAC	GCGTGGTGTGTTGTGGGTATC
Sost	GTGCCTCATCTGCCTACTTGTG	CGGTTCATGGTCTGGTTGTTCTC
Tnfa	CACGCTCTTCTGTCTACTGAACTTC	CTTGGTGGTTTGTGAGTGTGAGG
Il1b	TCGCAGCAGCACATCAACAAG	TCCACGGGAAAGACACAGGTAG
Il8	GAGCACTCCATAAGGCACAAA	ATGGTTCCTTCCGGTGGT

Biological Technology, China). Membranes were blocked with 5% bovine serum albumin (BSA) for 2 h, and then incubated overnight at 4°C with primary antibodies: β-catenin antibody (1:2000), Lamin B1 antibody (1:2000), Gapdh antibody (1:2000), MARCKS antibody (1:2000), or phospho-MARCKS (Ser159/163) (1:2000). After washing with PBST, membranes were incubated with the secondary antibody goat anti-rabbit IgG H&L (HRP) (1:5000) for 1.5 h at room temperature. Protein bands were visualized using enhanced chemiluminescence (ECL) reagent (Abbkine Scientific, China) and imaged using an ECL imager (CLINX Qinxiang Scientific, China). Band intensities were quantified using ImageJ and normalized to loading controls.[13]

2.10. Immunofluorescence detection of β-catenin nuclear translocation

Nuclear translocation of β-catenin was detected by immunofluorescence, as described.[25] Y4-GFP and Y4-Wnt7b cells were cultured in a 24-well plate for 24 h. Cells were fixed with 3.7% formaldehyde solution at room temperature for 3 min, permeabilized with 0.25% Triton X-100 for 30 min, and blocked with 1% BSA for 30 min. Cells were then incubated overnight at 4 °C with β-catenin antibody (1:100). After washing three times with PBS, cells were incubated with Cy3-labeled goat anti-rabbit IgG secondary antibody (1:200) for 60 min in the dark. Nuclei were counterstained with DAPI solution (200 μL per well) for 3 min. Images were acquired using a fluorescence microscope (Leica, Germany).

2.11. Induction of adipogenic differentiation

Adipogenic differentiation was induced as previously described.[24] Briefly, Y4-GFP or Y4-Wnt7b cells were cultured with ST2 cells at a 1:4 ratio in 12-well plates. Upon reaching confluency (typically after 3 days), the growth medium was replaced with adipogenic induction medium (DMEM supplemented with 10% FBS, 0.5 μM hydrocortisone, 0.5 mM IBMX, and 60 μM indomethacin). Cells were maintained in this medium for up to 7 days, with half of the medium replaced every 3 days, until lipid droplets were observed microscopically. Adipogenesis was visualized for 30 min using the Oil Red O staining kit according to the manufacturer's instructions. Lipid droplets were imaged using an inverted microscope (Nikon, Japan).

2.12. PCI3D module preparation

The PCI3D modules were biofabricated using a dual-nozzle 3D bioprinter (Sunpbiotech, China), incorporating PCL as structural support and cell-laden hydrogels containing functional MLO-Y4 and ST2 cells, as previously detailed.[23] Briefly, lyophilized GelMA was dissolved in α-MEM to prepare a 20% (w/v) GelMA solution containing 0.5% (w/v) LAP. A cell suspension containing 2×10^5 MLO-Y4 cells and 8×10^5 ST2 cells in 0.5 mL α-MEM was mixed with an equal volume of GelMA/LAP solution, resulting in a final bioink containing 10% (w/v) GelMA, 0.25% (w/v) LAP, and cells. The cell-laden bioink was loaded into a cooled syringe and printed using a cell-printing nozzle.

Simultaneously, PCL pellets were melted at 95°C for 30 min in a separate printing nozzle designed for thermoplastics. Melted PCL was printed at a speed of 2 mm/s to form a framework with a diameter of 400 μm and a spacing of 1100 μm. The cell-laden GelMA bioink was printed alongside the PCL strands at a speed of 5 mm/s (strand diameter: 300 μm; spacing: 500 μm). After printing each layer, the GelMA hydrogel was crosslinked under 405 nm blue light for 10 s. Printing was performed sequentially in three layers, with the PCL and cell-laden GelMA strands oriented perpendicularly between adjacent layers. The fabricated PCI3D modules were transferred to 6-well plates containing growth medium and cultured at 37°C with 5% CO_2.

2.13. Cell viability within PCI3D modules

Cell viability within PCI3D modules was quantified at Days 1, 4, and 7 of culture using a Calcein/ Propidium Iodide (PI) cell viability and cytotoxicity detection kit, as described previously.[23] Modules were washed with PBS and incubated in staining solution (prepared by diluting Calcein AM and PI stock solutions in assay buffer according to the kit instructions) for 30 min at 37 °C in the dark. Calcein AM stains live cells green, while PI stains dead cells red. Immediately after staining, the modules were imaged using an inverted fluorescence microscope (Leica, Germany). Cell viability was quantified using ImageJ software (64-bit, v1.46).

2.14. Cell proliferative activity within PCI3D modules

Cell proliferation in PCI3D modules was evaluated on Days 1, 4, and 7 using the CCK-8 assay kit, according to the manufacturer's instructions.[23] The PCI3D module was first washed with PBS, then cut into four pieces and placed in a 96-well plate. Subsequently, 90 μL of PBS and 10 μL of CCK-8 solution were added to each well and incubated for 2 h. The supernatant was then transferred to a new 96-well plate, and the absorbance was measured at 450 nm using the multi-function microplate reader (Thermo Fisher Scientific, USA).

2.15. 3D-BWBM system

The 3D-BWBM system was established to evaluate the protective effect of osteocytic Wnt7b against microgravity-impaired osteoblast differentiation. This system integrates the PCI3D system, which prints PCI3D modules[23] containing the biological microenvironment (Wnt7b-

overexpressing osteocytes in this study), with the R-approved microgravity-simulation system, RCCS™. The 3D-BWBM was set up in a CO_2 incubator.

In order to rapidly evaluate the effect of osteocytic Wnt7b on osteogenic differentiation under microgravity in a 3D environment closely resembling *in vivo* conditions,[26,27] we printed the PCI3D module and cut it into small modules about 5 × 5 mm^2 with optional compartments, allowing for installation within the high-aspect rotating vessel (HARV™) of the RCCS™. The HARV™ was filled with growth medium, carefully degassed to remove air bubbles, sealed with a plug at the filling port, and subsequently mounted onto the rotating base. To ensure clear experimental effects, prevent cell dislodgement, and maintain the module suspended at the center of the vessel, a rotational speed of 20–30 rpm/min was optimized for this experiment to simulate microgravity and low shear stress conditions.[28] Finally, RCCS™ was placed in a CO_2 incubator to culture the modules for 7 days, during which the medium was changed once.

2.16. Statistical analysis

GraphPad Prism 8.0.1 software was used for statistical analysis. Each experiment was repeated three times. Data were expressed as mean ± standard deviation. Differences in data between two groups were analyzed by *t*-test; differences between multiple groups were analyzed by one-way analysis of variance (ANOVA); and differences between groups with two or more independent variables were analyzed by two-way ANOVA. A *p*-value less than 0.05 indicates statistical significance.

3. Results

3.1. Osteocytic Wnt7b induces osteogenic differentiation of ST2 cells

We observed that mice with osteocyte-specific Wnt/β-catenin activation (daβcatOt) exhibited resistance to the induced bone loss in a tail suspension model simulating weightlessness. To investigate this phenomenon, we analyzed the expression of Wnt ligands in the long bones of daβcatOt mice and their cohort control mice (WT). We found that the expression levels of *Wnt3a*, *Wnt5a*, and *Wnt7b* were positively correlated with bone loss and bone protection in the microgravity environment (Figure 1A). To determine whether these three Wnt ligands possess a protective function against microgravity-induced bone loss in osteocytes, we established stable osteocyte cell line MLO-Y4 expressing Wnt5a, Wnt7b, and GFP (control), namely Y4-Wnt5a, Y4-Wnt7b, and Y4-GFP, respectively. RT-qPCR analysis revealed that Y4-Wnt5a and Y4-Wnt7b overexpressed their respective *Wnt5a* and *Wnt7b* mRNAs (Figure 1B). MLO-Y4 treated with Wnt3a-conditioned medium exhibited enhanced osteogenic differentiation-promoting activity.[29]

The prepared osteocyte cell lines were used as functional cells and co-cultured with effector cells, specifically bone marrow mesenchymal cells ST2, for 3 days (Figure 1C), followed by an assessment of their osteogenic differentiation activity. The co-culture cell ratio of MLO-Y4 to ST2 at 1:4 was selected (Figure S1, Supporting Information), consistent with previous reports indicating that osteogenic factors from osteocytes promote ST2 osteogenic differentiation through activation of the canonical Wnt signaling pathway.[25,30,31] Osteogenic differentiation, assessed by AP staining, displayed significantly increased staining intensity in the co-culture of Wnt3a-treated MLO-Y4 and Y4-Wnt7b groups, but no significant increase was observed in the Y4-Wnt5a co-culture group (Figure 1D). The Y4-GFP co-culture group exhibited no significant difference compared to the MLO-Y4 co-culture group treated with the Wnt3a control medium (L-ctrl). Consistent with the staining results, Y4-Wnt7b and Y4-Wnt3a significantly promoted osteogenic differentiation, with robust increases in AP biochemical activity compared to their respective controls, Y4-GFP and Y4-L-ctrl (Figure 1E).

However, given that the osteogenic activity of Wnt3a can be inhibited by the Wnt/β-catenin antagonist ICG-001[32] and that sclerostin produced by microgravity also inhibits the canonical Wnt signaling pathway, we focused on Wnt7b as a potential strategy to bypass sclerostin inhibition under microgravity conditions. Furthermore, RT-qPCR analysis revealed that the Y4-Wnt7b co-culture group significantly upregulated the expression of osteoblast marker genes (*Alpl, Col1a1, Ibsp,* and *Bglap*) in ST2 cells (Figure 1F). To verify whether the osteocyte-mediated osteogenic differentiation of ST2 cells in the co-culture system was exclusively derived from ST2 cells, we then examined the AP expression of Y4-GFP and Y4-Wnt7b cells, respectively. The AP staining results showed that the intensity of AP staining of Y4-Wnt7b itself and Y4-GFP cells was significantly weaker than that in the ST2 cells cocultured with L-ctrl medium-treated MLO-Y4 and Y4-GFP (Figure S2A, Supporting Information). Also, the mRNA levels of osteoblast marker genes *Alpl*, *Ibsp*, and *Bglap* were comparable to those of Y4-GFP cells in Y4-Wnt7b cells (Figure S2B, Supporting Information), suggesting that Wnt7b hardly altered the expression of osteoblast marker genes in MLO-Y4 cells. Finally, we assessed the effect of osteocyte Wnt7b on mineralization. ARS staining demonstrated that the mineralized nodules formed in the Y4-Wnt7b co-culture group were larger, denser, and had 1.4 times more calcium deposition than those in the Y4-GFP co-culture group (Figure 1G).

Therefore, we will conduct further studies on the force-sensitive and functional bone cell Wnt7b, which actively counteracts microgravity-induced impairment of osteoblast differentiation.

3.2. Osteocytic Wnt7b activates the PKCδ pathway of Wnt noncanonical signaling to promote osteogenic differentiation

To determine whether osteocytic Wnt7b signals through the canonical Wnt pathway, we assessed β-catenin protein levels in Y4-Wnt7b cells, as β-catenin is a central mediator of canonical signaling.[13] Western blot analysis of cytoplasmic and nuclear fractions revealed no significant difference in β-catenin levels compared to Y4-GFP controls (Figure 2A). Furthermore, immunofluorescence staining with an anti-β-catenin antibody demonstrated no observable translocation of β-catenin from the cytoplasm to the nucleus in Y4-Wnt7b cells relative to Y4-GFP cells (Figure 2B). Moreover, at concentrations below 10 μM, iCRT-14 (the canonical Wnt signaling antagonist) did not attenuate Y4-Wnt7b-induced osteoblast differentiation of ST2 cells, as measured by AP staining and its biochemical activity assays (Figure S3A and B, Supporting Information). Similarly, iCRT-14 did not alter the expression of the canonical Wnt target gene *Axin2* compared to the DMSO control (Figure S3C, Supporting Information). These findings indicate that osteocytic Wnt7b does not activate the canonical Wnt signaling pathway.

Given our previous reports that Wnt7b activates noncanonical pathways involving mTORC1[14] and PKCδ[13] in osteoblasts to promote bone formation, we next investigated these possibilities in our osteocyte model. Treatment with the mTORC1-specific inhibitor rapamycin[33] in the co-culture of Y4-Wnt7b and ST2 cells for 3 days displayed no significant inhibition of AP activity. In contrast, rapamycin effectively inhibited osteoblast differentiation induced by Wnt3a-treated MLO-Y4 cells (Figure S4, Supporting Information). This suggests that mTORC1 signaling is not essential for osteocytic Wnt7b-mediated osteogenesis.

Finally, we tested the involvement of PKCδ signaling using its selective inhibitor Rottlerin.[34] Firstly, we tested the effect of different concentrations of Rottlerin on Wnt7b-induced osteogenic differentiation. AP staining revealed that treatment with 1 μM Rottlerin significantly reduced the differentiation function of Y4-Wnt7b cells (Figure 2C). Furthermore, Rottlerin inhibited the phosphorylation of the myristoylated alanine-rich C-kinase substrate (MARCKS), which is a well-established marker of PKC activation.[35] Western blot analysis demonstrated that Y4-Wnt7b cells exhibited increased levels of p-MARCKS (Ser159/163) compared to controls. Treatment of Y4-Wnt7b cells with 1 μM Rottlerin significantly reduced p-MARCKS levels (Figure 2D). Functionally, 1 μM Rottlerin completely inhibited osteoblast differentiation in ST2 cells co-cultured with Y4-Wnt7b cells, as observed in AP staining and its biochemical activity assays (Figure 2E and F), significant downregulation of osteoblast marker genes (*Alpl, Col1a1, Ibsp*) via qPCR (Figure 2G), and a marked 1.4-fold reduction in osteocytic Wnt7b-induced mineralization by ARS staining (Figure 2H).

Collectively, these results demonstrate that osteocytic Wnt7b promotes osteogenic differentiation of ST2 cells primarily through activation of the PKCδ-mediated noncanonical Wnt signaling pathway, rather than through canonical Wnt or mTORC1 signaling.

3.3. Osteocytic Wnt7b-PKCδ pathway inhibits adipogenic differentiation

To investigate whether osteocytic Wnt7b inhibits adipogenic differentiation, we co-cultured Y4-Wnt7b and ST2 cells (1:4 ratio) in adipogenic medium for 7 days. While abundant lipid droplets formed in ST2 cells co-cultured with Y4-GFP controls, visualized by Oil Red O staining (Figure 3A), significantly fewer droplets were observed in the Y4-Wnt7b group. Furthermore, osteocytic Wnt7b downregulated the expression of key adipogenic transcription factors PPARγ (*Pparg*) and C/EBPα (*Cebpa*) (Figure 3B).

Next, we investigated whether inhibition of PKCδ signaling could restore the adipogenic differentiation of ST2 cells by using Rottlerin in the co-culture system. After 7 days of adipogenic induction, lipid droplet accumulation increased with Rottlerin concentration, largely reaching control (Y4-GFP) levels at 1 μM (Figure 3A). However, the lipid droplets were smaller and denser, which may be due to the continued inhibition of Wnt7b-PKCδ signaling by Rottlerin, thereby preventing the formation of larger lipid droplets. Consistent with this observation, 2 μM Rottlerin restored *Pparg* and *Cebpa* expression to control levels (Figure 3B).

The above results indicated that Rottlerin reverses the osteocytic Wnt7b-mediated inhibition of adipogenesis, suggesting that the Wnt7b-PKCδ signaling axis in osteocytes plays an important role in the negative regulation of adipogenesis.

3.4. Construction of Y4-Wnt 7b PCI3D modules

We fabricated 3D scaffolds using our in-house developed PCI3D system,[23] simultaneously printing PCL frameworks and cell-laden hydrogel bundles containing either Y4-GFP or Y4-Wnt7b cells mixed with ST2 cells at a 1:4 ratio (Figure 4A). GelMA hydrogel served as the bioink for the cell bundles. Utilizing its temperature-dependent viscosity, GelMA was uniformly extruded at 25°C using a

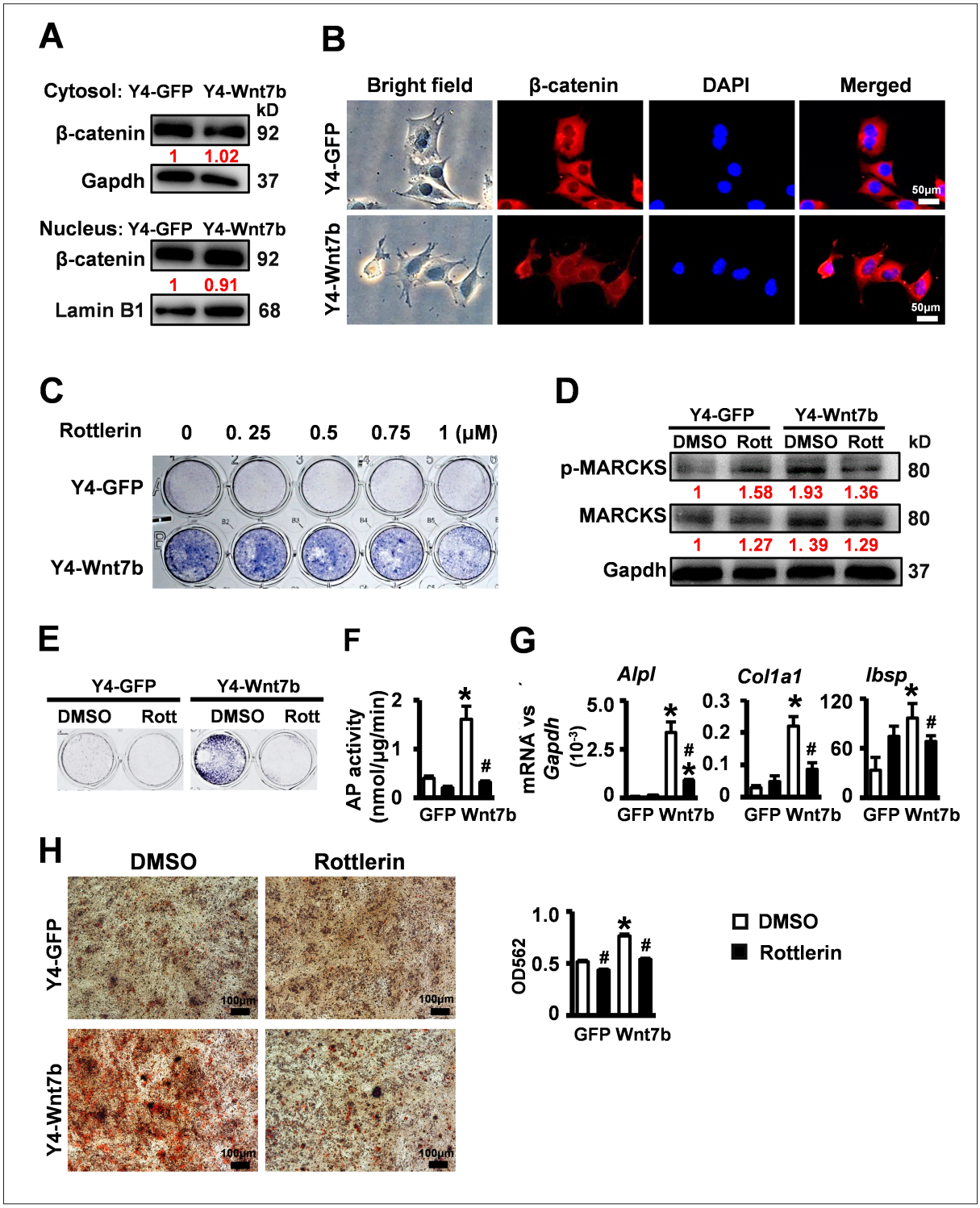

Figure 2. Osteocytic Wnt7b activates the PKCδ pathway to promote osteogenic differentiation. (A) Western blot analysis of β-catenin levels in cytoplasmic and nuclear extractions of Y4-Wnt7b and Y4-GFP cells. (B) Immunofluorescence staining of β-catenin (red) and nuclei (DAPI, blue) in Y4-Wnt7b cells. Scale bar = 50 μm. (C) AP staining in ST2 cells co-cultured with Y4-Wnt7b in different concentrations of Rottlerin. (D) Western blot analysis of phospho-MARCKS in the lysates of Y4-Wnt7b and Y4-GFP cells. (E–G) The effect of PKCδ signaling on osteocytic Wnt7b-induced osteoblast differentiation of ST2 cells was examined by AP staining (E), AP biochemical activity assay (F), and qPCR of osteoblast marker genes (G). (H) Alizarin Red S staining of mineralized nodulesof PKCδ signaling on the mineralization of osteocytic Wnt7b-induced osteoblast. Scale bar = 100 μm. *$p < 0.05$ versus Y4-GFP, #$p < 0.05$ versus DMSO control ($n = 3$) for panels F, G, H. Abbreviations: Bright field; DMSO, dimethyl sulfoxide.

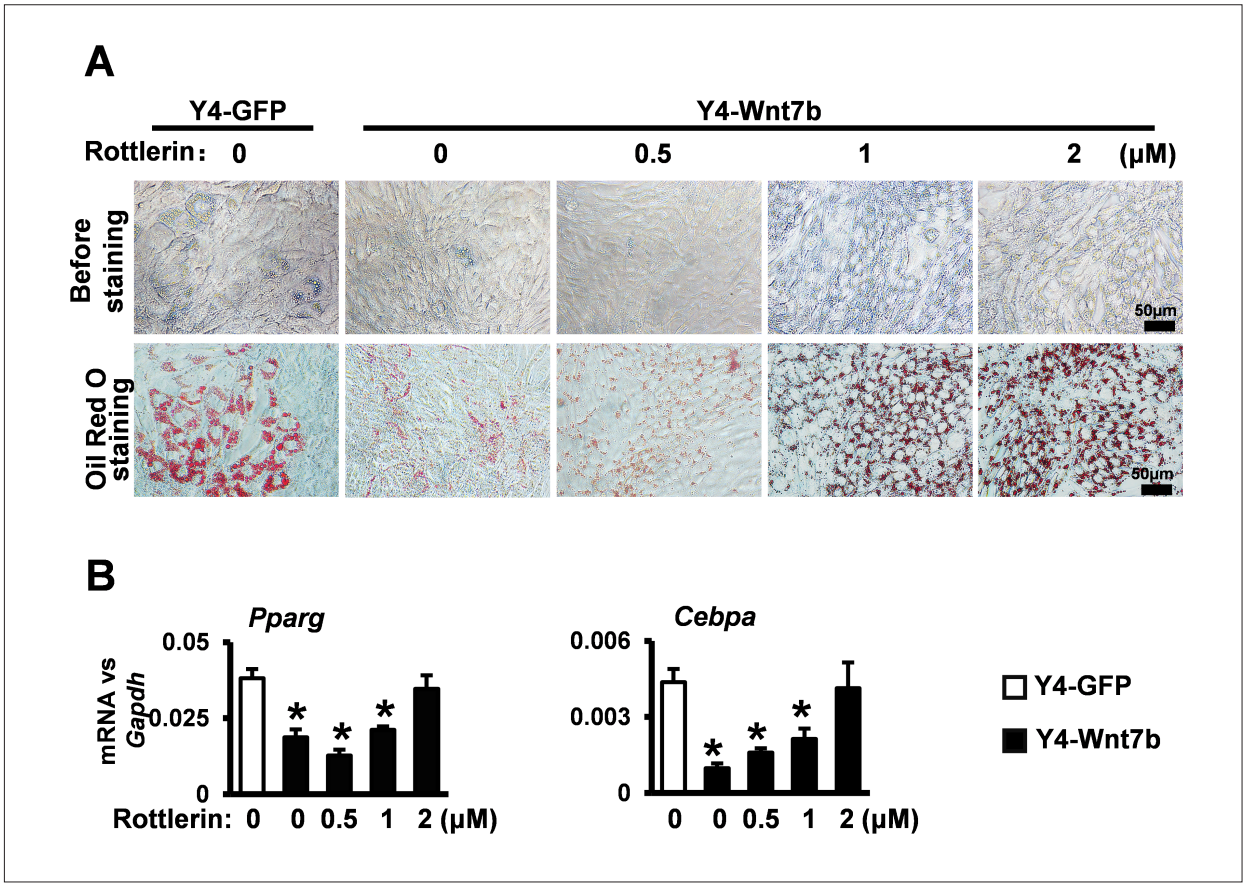

Figure 3. Osteocytic Wnt7b inhibits adipogenic differentiation via PKCδ. (A) Light microscopy and Oil Red O staining of lipid droplets in ST2 cells co-cultured with Y4-Wnt7b, with or without Rottlerin treatment (0.5–2 μM) for 7 days in adipogenic medium. Scale bars: 50 μm. (B) Expression of adipogenic transcription factors (*Pparg*, *Cebpa*) ($n = 3$); $^*p < 0.05$ versus Y4-GFP.

pneumatic syringe with a 300-μm nozzle diameter. PCL bundles and hydrogel bundles were printed in parallel with interconnecting 400-μm tunnels to facilitate nutrient transport and metabolite exchange. Y4-Wnt7b modules were fabricated by alternating printing cycles with blue-light crosslinking. The resulting modules exhibited stable mechanical support and interconnected pore architecture conducive to mass transport.

We first assessed the impact of Y4-Wnt7b on cell viability and proliferation within the PCI3D modules. Calcein AM/PI staining performed after 1, 4, and 7 days of culture revealed high cell viability over time (Figure 4B). Quantitative analysis (ImageJ) confirmed cell survival rates exceeding 97% in both Y4-GFP and Y4-Wnt7b groups throughout the 7-day period (Figure 4C). CCK-8 proliferation assays demonstrated steady cell growth within the modules. Notably, the Y4-Wnt7b group exhibited significantly higher proliferative activity compared to the Y4-GFP control group at Days 4 and 7 (Figure 4D). These results indicate that the PCI3D modules provide a supportive microenvironment for sustained cell survival and proliferation.

3.5. Osteocytic Wnt7b promotes osteogenic differentiation of ST2 cells in PCI3D modules

To assess the function of osteocytic Y4-Wnt7b in promoting osteogenic differentiation within a simulated *in vivo* 3D environment, we utilized PCI3D modules seeded with ST2 cells. Y4-Wnt7b- or Y4-GFP-expressing PCI3D modules were co-cultured with ST2 cells in growth medium for 7 or 14 days. Compared to the Y4-GFP controls, the Y4-Wnt7b group exhibited increased AP staining intensity (Figure 5A) and significantly enhanced AP activity (Figure 5B), indicating that Wnt7b potently augmented ST2 cell osteogenic differentiation within the 3D modules. Consistent with this, qPCR analysis revealed that Y4-Wnt7b significantly upregulated the expression of key osteogenic marker genes (*Alpl*, *Col1a1*, *Runx2*) at both

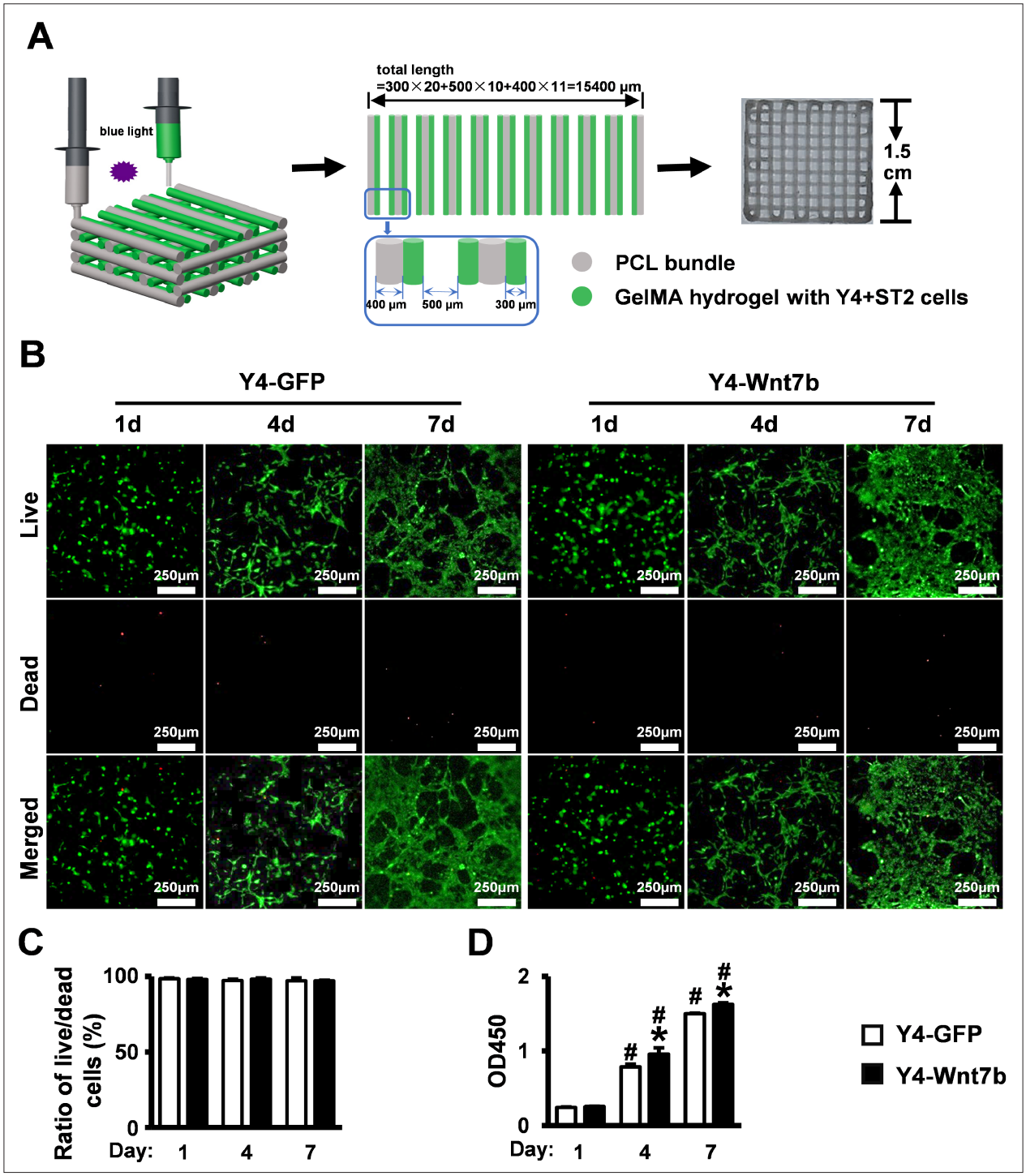

Figure 4. Cell viability and proliferation in 3D-printed PCI3D modules. (A) Schematic of PCI3D module fabrication: PCL bundles (gray) and cell-laden GelMA hydrogels (green) were alternately printed. (B) Calcein AM (live, green)/PI (dead, red) staining of Y4-Wnt7b and ST2 cells after 1, 4, and 7 days of co-culture. Scale bar: 250 μm. (C) Live/dead cell ratio was analyzed by ImageJ. (D) CCK-8 assay for proliferative activity. *$p < 0.05$ versus Y4-GFP; #$p < 0.05$ versus Day 1 by two-way ANOVA ($n = 3$). Abbreviations: ANOVA, analysis of variance; Calcein AM, calcein acetoxymethyl ester; GelMA, gelatin methacryloyl; PCL, poly-ε-caprolactone; PI, propidium iodide.

time points, with expression levels further elevated at Day 14 (Figure 5C).

We next evaluated the effect of Y4-Wnt7b on mineralization within the PCI3D modules. Following 7 days in growth medium, the modules were cultured in osteogenic medium containing ascorbic acid and β-glycerophosphate disodium for an additional 14 days. ARS staining demonstrated a marked increase in mineralized nodule formation in the Y4-Wnt7b modules compared to Y4-GFP controls, with a corresponding 1.8-fold increase in calcium deposition (Figure 5D). This further confirmed the potent role of osteocytic Wnt7b in driving osteogenic differentiation and matrix mineralization within the 3D environment.

Furthermore, analysis of adipogenic potential revealed that Y4-Wnt7b significantly downregulated the expression of adipogenic transcription factors (*Pparg*, *Cebpa*, *Fabp4*) compared to controls (Figure 5E). This suggests that Wnt7b may also inhibit adipogenic differentiation within the simulated *in vivo* environment provided by the PCI3D modules.

3.6. Osteocytic Wnt7b promotes osteoblast differentiation independent of microgravity-induced sclerostin production

We found that osteocytic Wnt7b significantly promotes ST2 cell osteogenic differentiation and mineralization through the Wnt noncanonical signaling pathway in both 2D and 3D cultures. To test whether this mechanism functions in weightless environments, we built the 3D-BWBM system that simulates a microgravity biological microenvironment using RCCS™ (Figure 6A). The system enables rapid examination of the effects of simulated *in vivo* Wnt7b on osteoblast differentiation within a 3D-printed scaffold. After 7 days of cultivation in HARV™, MLO-Y4 cells expressed higher levels of myocyte enhancer factor 2C (*Mef2c*), which can activate the expression of *Sost*, leading to sclerostin production.[36] The qPCR results demonstrated that the mRNA levels of both *Sost* and *Mef2c* were significantly upregulated (Figure 6B), indicating that the microgravity conditions were successfully simulated in osteocytes.

Mechanosensory osteocytes upregulate the expression of *Sost*/sclerostin under mechanical unloading[11,37,38] and downregulate it under mechanical loading,[11,37] respectively. Sclerostin is known to bind to Lrp5/6 and inhibit the Wnt canonical signaling pathway,[39] thereby suppressing bone formation both *in vitro* and *in vivo*. We placed PCI3D modules into HARV™ and suspended them for 7 days. Meanwhile, under microgravity conditions, osteocytic Wnt7b significantly maintained and even enhanced osteoblast differentiation of ST2 cells, as observed by AP staining and activity assays, compared to Y4-GFP controls (Figure 7A and B). The qPCR results revealed that Y4-Wnt7b significantly upregulated the expression of osteoblast marker genes *Alpl*, *Ibsp*, *Col1a1*, *Bglap*, and *Sp7* (Figure 7). These data confirm that osteocytic Wnt7b continues to promote osteogenic differentiation of ST2 cells under microgravity conditions, suggesting a strong protective effect of Wnt7b against weightlessness-induced bone loss.

However, osteocytic Wnt7b had the least effect on adipogenesis compared with the Y4-GFP group, with no significant difference in the expression of adipogenic transcription factors *Pparg*, *Cebpa*, or *Fabp4*, all of which tended to decrease under microgravity conditions (Figure 7D).

4. Discussion

Our study demonstrated that osteocyte-derived Wnt7b effectively promotes osteogenic differentiation of bone marrow stromal cells (ST2) and protects against microgravity-induced impairment of osteogenesis. This protective effect stems from Wnt7b's unique ability to activate the sclerostin-independent Wnt noncanonical PKCδ signaling pathway. We further established a functionalized 3D-bioprinted osteocyte niche (PCI3D module) and integrated it with a simulated microgravity platform (3D-BWBM) to validate Wnt7b's efficacy under conditions mimicking spaceflight.

The impetus for this investigation arose from our observation that elevated Wnt7b expression correlates with preserved bone mass in osteocyte-specific β-catenin activated (daβcat^{Ot}) mice subjected to tail suspension, a model of disuse osteoporosis and simulated microgravity. We mechanistically demonstrated that osteocytic Wnt7b potently induces osteoblast differentiation and mineralization in co-cultured ST2 cells, while concurrently suppressing adipogenesis by downregulating key adipogenic transcription factors *Pparg* and *Cebpa*. Critically, the specific PKCδ inhibitor Rottlerin inhibited Wnt7b-induced osteogenesis and reversed its inhibition of adipogenesis in ST2 cells (Figure 7E), unequivocally establishing the PKCδ pathway as the central mediator of Wnt7b's dual function. This positions Wnt7b as a potent intrinsic physiological osteogenic microenvironmental factor (POME) and a compelling candidate for BTE applications.

Beyond sclerostin upregulation, our gene expression analysis within the 3D-BWBM system confirmed a comprehensive microgravity response. We observed the expected upregulation of *Sost* and its transcriptional

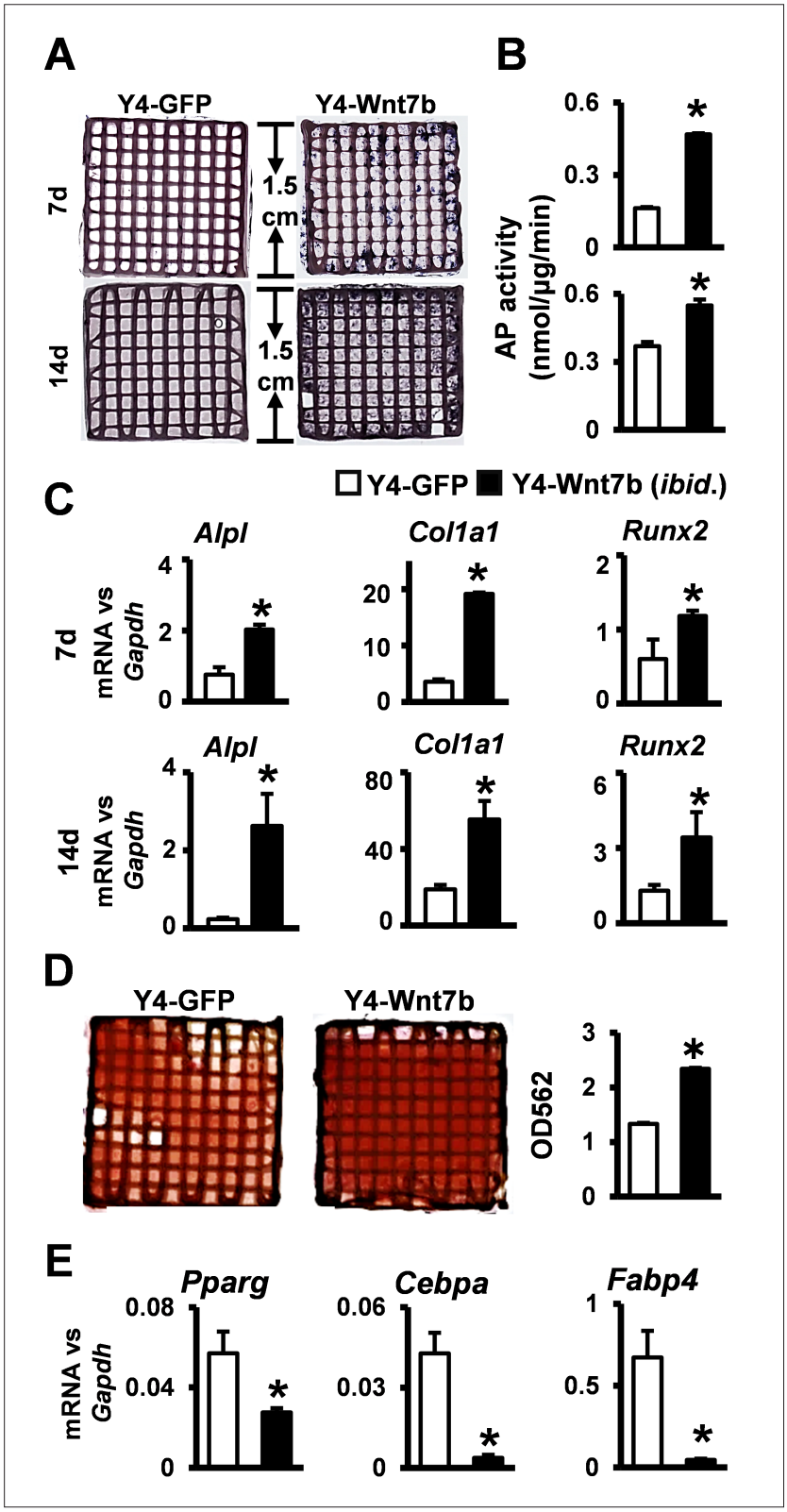

Figure 5. Osteogenic and anti-adipogenic effects of osteocytic Wnt7b in 3D modules. (A–C) AP staining (A), AP activity (B), and osteoblast marker gene expression (C) of Y4-Wnt7b on osteoblast differentiation of ST2 cells in PCI3D modules cultured for 7 and 14 days. (D) Alizarin Red S staining of mineralization. (E) Adipogenic gene expression (*Pparg, Cebpa, Fabp4*). *$p < 0.05$ versus Y4-GFP by Student's *t*-test; $n = 3$.

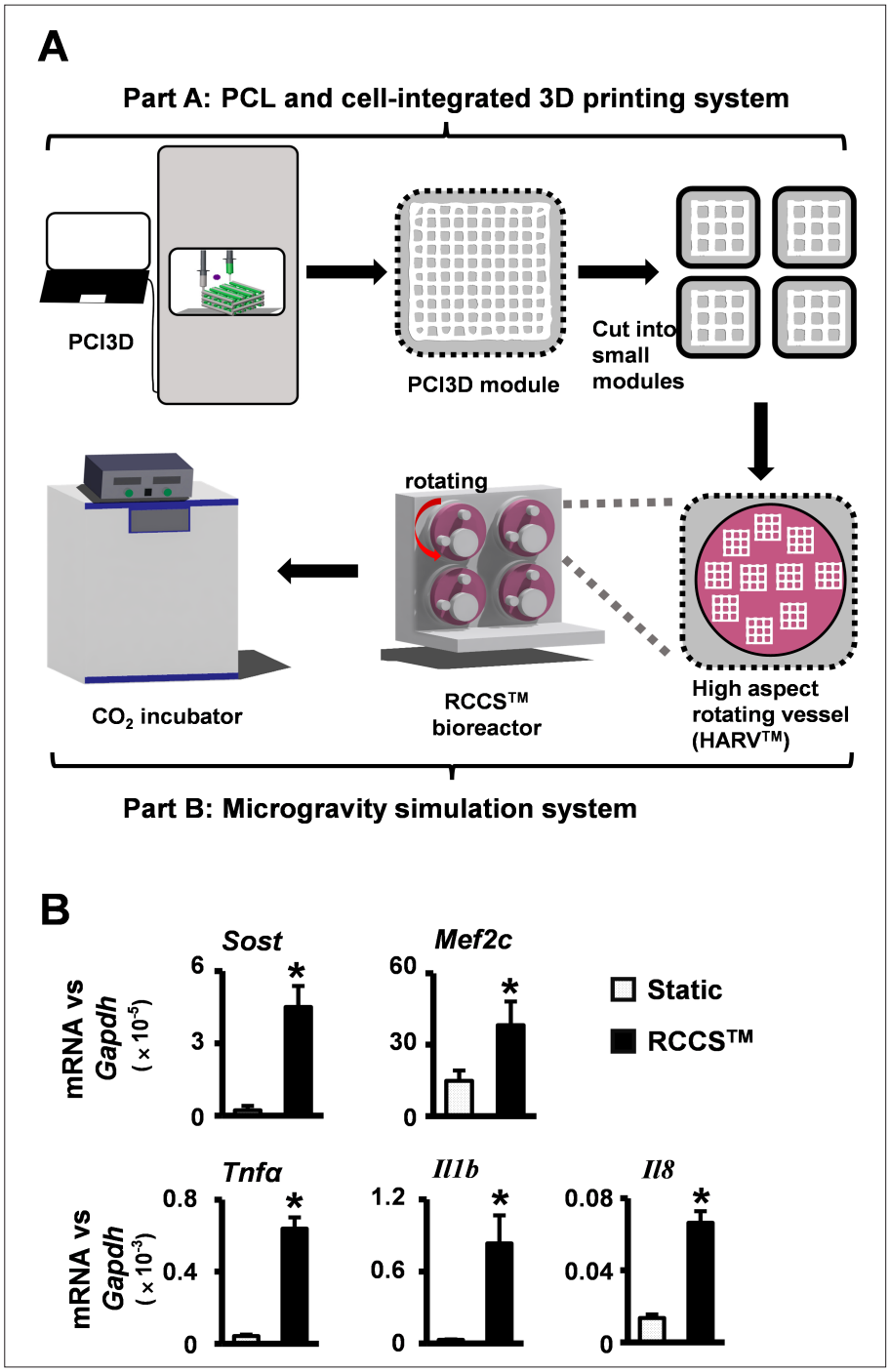

Figure 6. The 3D-BWBM system for microgravity simulation. (A) Diagram of the 3D-BWBM system combining PCI3D printing (Part A) and NASA's RCCS™ bioreactor (Part B). (B) Reverse transcription quantitative polymerase chain reaction (RT-qPCR) results of Sost (sclerostin), Mef2c, Il1b, Tnfa, and Il8 in PCI3D modules under static or microgravity conditions. *$p < 0.05$ versus Y4-GFP by Student's *t*-test; $n = 3$. Abbreviations: 3D-BWBM, 3D biomimetic weightless bio-microenvironmental system; NASA, National Aeronautics and Space Administration; PCI3D, PCL and cell-integrated 3D-printed; RCCS™, Rotary Cell Culture System; RT-qPCR, reverse transcription quantitative polymerase chain reaction.

regulator *Mef2c*.[36] Furthermore, elevated pro-inflammatory cytokines (*Tnfa*, *Il1b*) are consistent with the inflammatory and catabolic state triggered by microgravity,[40] potentially contributing to enhanced osteoclastogenesis, as evidenced by an increased *Rankl/Opg* ratio. The disruption of mechanotransduction cascades in microgravity likely impairs normal osteocyte function, biasing stromal cell fate towards adipogenesis at the expense of osteogenesis.[41] Thus, the 3D-BWBM system robustly recapitulates key

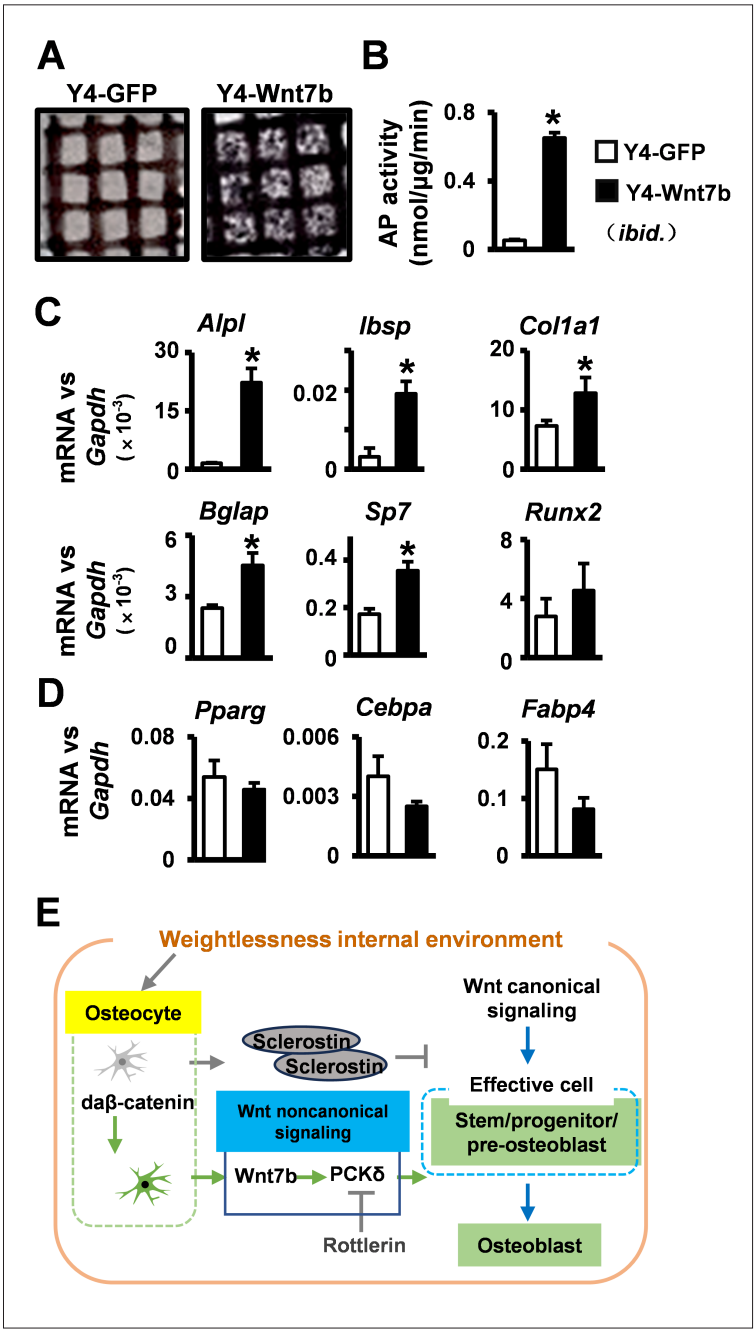

Figure 7. Osteocytic Wnt7b protects osteogenesis under microgravity. (A–C) Alkaline phosphatase (AP) staining (A), AP activity (B), and osteoblast marker gene expression (C) in PCI3D modules cultured in 3D-BWBM for 7 days. (D) Adipogenic gene expression under microgravity conditions. (E) Proposed model: Wnt7b-PKCδ signaling bypasses sclerostin-mediated inhibition of canonical Wnt to promote osteogenesis. *$p < 0.05$ vs. Y4-GFP; $n = 3$. Abbreviation: 3D-BWBM, 3D biomimetic weightless biomicroenvironmental system.

pathophysiological features of weightlessness-induced bone loss.

Osteocytic Wnt7b represents a novel POME acting through the Wnt noncanonical PKCδ pathway, distinguishing it from our previous reports on osteogenic microenvironments, such as osteocyte-activated canonical Wnt signaling,[25,30,31] decellularized matrix,[29] Dll4,[23] and BMP7,[42] all of which operate through different mechanisms. Importantly, Wnt7b-PKCδ signaling bypasses sclerostin-mediated inhibition of the canonical Wnt pathway, a major limitation of current anabolic strategies like Romosozumab (sclerostin antibody) and potentially Teriparatide (parathyroid hormone, PTH1-34).[43] While the anabolic mechanism of abaloparatide (parathyroid hormone-related protein, PTHrP) remains unclear, our findings highlight Wnt noncanonical signaling—particularly via osteocytic Wnt7b-PKCδ—as a previously unexplored and highly promising target for counteracting disuse osteoporosis. Currently, no therapies specifically target Wnt noncanonical signaling for weightlessness-induced bone loss, nor utilize osteocytes engineered with this pathway as functional cells within 3D constructs to promote osteogenesis under microgravity.

While our data robustly support Wnt7b's protective role against microgravity-impaired osteogenesis via sclerostin-independent PKCδ activation, definitive proof of causality necessitates further *in vivo* studies. Conditional knockout of Wnt7b specifically in the osteocytes of daβcat^{Ot} mice, or its neutralization via antibodies, will establish whether Wnt7b is indispensable for the observed bone-sparing effects. We are currently designing these experiments using tail-suspended mouse models. Additionally, testing if osteocyte-specific Wnt7b overexpression alone (without concomitant β-catenin activation) replicates the protective phenotype in wild-type mice will further isolate its intrinsic therapeutic potential.

Both Wnt/β-catenin and noncanonical pathways (especially the Wnt-Ca^{2+} pathway) generally promote osteoblastogenesis while inhibiting adipogenesis.[44] PKC isoforms exhibit complex, sometimes opposing, roles in adipogenesis.[45–47] Fleming et al.[48] demonstrated that PKC-α, -δ, and -μ inhibit adipogenesis, while PKC-ε promotes it. Our results demonstrate that osteocytic Wnt7b inhibits adipogenesis by downregulating the transcription of the adipogenic transcription factors *Pparg* and *Cebpa* through PKCδ signaling under 2D and simulated 3D conditions. Although microgravity typically enhances adipogenesis in human mesenchymal stem cells,[34] the expression of adipogenic factors tended to decrease in our 3D-BWBM system containing Wnt7b osteocytes. This suggests that the dual function of the Wnt7b-PKCδ axis—of promoting osteogenesis while suppressing adipogenesis—may be particularly well-suited for preventing the skewed lineage commitment characteristic of weightlessness-induced bone loss.

Interestingly, unlike Wnt canonical signaling, osteocytic Wnt7b did not significantly alter the expression of osteoclast regulators (*Rankl, Opg,* and *Rankl/Opg* ratio) under static culture. However, microgravity itself robustly increased the *Rankl/Opg* ratio. Intriguingly, osteocytic Wnt7b further elevated this ratio to control Y4-GFP under microgravity (Figure S5, Supporting Information), suggesting that Wnt7b may paradoxically enhance osteoclast differentiation in disuse conditions. While counterintuitive for an anabolic process, enhanced bone resorption could potentially contribute to bone remodeling by recruiting mesenchymal stem cells to resorption sites, ultimately promoting subsequent bone formation.[49] The net effect *in vivo* warrants further investigation.

Current countermeasures against spaceflight bone loss, including exercise, nutrition,[50] and drugs (e.g., PTH[51]), face significant challenges in terms of their efficacy and practicality in microgravity. Antibodies targeting sclerostin displayed promise but can only partially mitigate bone loss in partially weight-bearing mice.[52] Crucially, sclerostin production persists during prolonged spaceflight or bed rest, raising concerns about the long-term efficacy and potential side effects of continuous antibody administration. Clinically effective PTH exhibits region-specific and load-dependent responses under weightlessness conditions,[51] and an ultra-high dose (80 μg/kg/day) of PTH was required for protection in one study,[39] posing osteosarcoma risks.[53] PTHrP promotes bone formation but may not directly drive osteogenic differentiation of progenitor cells.[54] Therefore, novel anabolic strategies are urgently needed. Wnt7b, acting independently of *Sost*/sclerostin and effectively promoting osteogenesis even in its presence, emerges as a highly promising candidate for protecting weightlessness-induced bone loss.

The 3D-BWBM system represents a significant technological innovation, integrating our in-house PCI3D bioprinting with the established RCCS™ bioreactor. This system enables rapid assessment of potential bone homeostasis regulators under simulated microgravity within a biomimetic 3D microenvironment. Current microgravity tissue engineering models, whether 2D[55] or 3D,[56–59] often lack the interconnected tunnel structures essential for efficient nutrient/oxygen/metabolite exchange, limiting cell viability, and function deep within constructs. Unlike conventional BTE scaffolds, where cell activity is often confined to surfaces,[60] our PCI3D module features precisely printed, uniform tunnels

(~500 μm diameter), facilitating excellent nutrient/metabolite transport, and closely mimicking the *in vivo* physiological conditions.[23] The RCCS™ rotation provides simulated microgravity while ensuring sufficient mass transport for 3D tissue culture.[59] Using this advanced system, we confirmed that osteocytic Wnt7b robustly promotes osteogenic differentiation of stromal cells under microgravity, consistent with our *in vivo* finding of increased lumbar BMD in protected mice.

Furthermore, advances in BTE and 3D printing enable precise control over implant shape and structure.[61,62] Integrating bioactive microenvironments with printing materials is key to enhancing implant functionality.[63,64] Bioprinting combined with specific cellular microenvironments offers a powerful strategy for creating "smart" constructs that mimic the microenvironment to support stem cell proliferation, migration, and differentiation.[65] Our approach of co-printing Wnt7b-expressing osteocytes with stromal cells within a PCL-GelMA scaffold not only ensured excellent cell survival and proliferation but also effectively supported osteogenic differentiation and mineralization. This underscores the significant potential of osteocytic Wnt7b as a molecular target and bioactive component for: (i) reconstructing bone integrity in astronauts, long-term bedridden patients, or those with paralysis to prevent disuse osteoporosis; and (ii) serving as a novel bioactive material for repairing critical-sized bone defects.

5. Conclusion

In this study, we demonstrated that osteoblast-derived Wnt7b effectively counteracted microgravity-induced bone loss by activating the sclerostin-independent PKCδ pathway, which promotes osteogenesis while inhibiting adipogenesis in bone marrow stromal cells. Through innovative 3D bioprinting technology, we developed a functionalized osteocyte niche (PCI3D) and validated its efficacy in a simulated microgravity system (3D-BWBM), confirming that Wnt7b exerts a protective effect towards weightlessness-induced bone loss. Our findings highlight Wnt7b-PKCδ signaling as a novel target for the treatment of disuse osteoporosis and establish a scalable bioengineering strategy for bone regeneration in extreme environments. Future *in vivo* studies will further elucidate its translational potential in spaceflight and clinical applications.

Acknowledgments

The authors are grateful to Lynda Bonewald for kindly providing the MLO-Y4 cell line.

Funding

This work was supported by the National Natural Science Foundation of China (grant numbers: 82471909, 81672118, and 32101053) and the Chongqing Natural Science Foundation (grant numbers: CSTB2022NSCQ-LZX0048 and CSTB2023NSCQ-MSX0424).

Conflict of interest

The authors declare they have no competing interests.

Author contributions

Conceptualization: Xing Liu, Xiaolin Tu
Formal analysis: Jinling Zhang, Pengtao Wang, Xiaoling Chen, Yangxi Liu, Bo He
Investigation: Jinling Zhang, Pengtao Wang, Xiaoling Chen, Saima Khan, Haiping Ouyang
Methodology: Jinling Zhang, Pengtao Wang
Writing–original draft: Jinling Zhang, Pengtao Wang, Xing Liu
Writing–review & editing: Jinling Zhang, Pengtao Wang, Xian Li, Xing Liu, Xiaolin Tu

Ethics approval and consent to participate

All animal procedures were approved by the Institutional Animal Care and Use Committee of Chongqing Medical University (IACUC-CQMU-2024-0277).

Consent for publication

Not applicable.

Availability of data

Data presented in this study are available upon request from the corresponding authors.

Further disclosure

This study was presented orally by Jinling Zhang at the 2023 China Biomaterials Conference in October 2023.

References

1. McCarthy ID. Fluid shifts due to microgravity and their effects on bone: a review of current knowledge. *Ann Biomed Eng.* 2005;33:95-103.
doi: 10.1007/s10439-005-8967-6

2. Lang T, LeBlanc A, Evans H, Lu Y, Genant H, Yu A. Cortical and trabecular bone mineral loss from the spine and hip in long-duration spaceflight. *J Bone Miner Res.* 2004;19:1006-1012.
doi: 10.1359/jbmr.040307

3. Durnova G, Kaplansky A, Morey-Holton E. Histomorphometric study of tibia of rats exposed aboard American spacelab life sciences 2 shuttle mission. *J Gravit Physiol.* 1996;3:80-81.

4. Carmeliet G, Bouillon R. The effect of microgravity on morphology and gene expression of osteoblasts in vitro. *Faseb J.* 1999; 13(Suppl):S129-S134. doi: 10.1096/fasebj.13.9001.s129

5. Smith SM, Wastney ME, O'Brien KO, et al. Bone markers, calcium metabolism, and calcium kinetics during extended-duration space flight on the mir space station. *J Bone Miner Res.* 2005; 20:208-218. doi: 10.1359/jbmr.041105

6. Vico L, Hargens A. Skeletal changes during and after spaceflight. *Nat Rev Rheumatol.* 2018;14: 229-245. doi: 10.1038/nrrheum.2018.37

7. Robling AG, Bonewald LF. The osteocyte: new insights. *Annu Rev Physiol.* 2020;82:485-506. doi: 10.1146/annurev-physiol-021119-034332

8. Delgado-Calle J, Bellido T. The osteocyte as a signaling cell. *Physiol Rev.* 2022;102:379-410. doi: 10.1152/physrev.00043.2020

9. Spatz JM, Wein MN, Gooi JH, et al. The Wnt inhibitor sclerostin is up-regulated by mechanical unloading in osteocytes in vitro. *J Biol Chem.* 2015;290:16744-16758. doi: 10.1074/jbc.M114.628313

10. Lin C, Jiang X, Dai Z, et al. Sclerostin mediates bone response to mechanical unloading through antagonizing Wnt/beta-catenin signaling. *J Bone Miner Res.* 2009;24:1651-1661. doi: 10.1359/jbmr.090411

11. Tu X, Rhee Y, Condon KW, et al. Sost downregulation and local Wnt signaling are required for the osteogenic response to mechanical loading. *Bone.* 2012;50:209-217. doi: 10.1016/j.bone.2011.10.025

12. Bloomfield SA, Martinez DA, Boudreaux RD, Mantri AV. Microgravity stress: bone and connective tissue. *Compr Physiol.* 2016;6:645-686. doi: 10.1002/cphy.c130027

13. Tu X, Joeng KS, Nakayama KI, et al. Noncanonical Wnt signaling through G protein-linked PKCdelta activation promotes bone formation. *Dev Cell.* 2007;12:113-127. doi: 10.1016/j.devcel.2006.11.003

14. Chen J, Tu X, Esen E, et al. WNT7B promotes bone formation in part through mTORC1. *PLoS Genet.* 2014;10:e1004145. doi: 10.1371/journal.pgen.1004145

15. Cui Y, Liu W, Zhao S, Zhao Y, Dai J. Advances in microgravity directed tissue engineering. *Adv Healthc Mater.* 2023;12:e2202768. doi: 10.1002/adhm.202202768

16. Bradbury P, Wu H, Choi JU, et al. Modeling the impact of microgravity at the cellular level: implications for human disease. *Front Cell Dev Biol.* 2020;8;96. doi: 10.3389/fcell.2020.00096

17. Silvani G, Basirun C, Wu H, et al. A 3D-bioprinted vascularized glioblastoma-on-a-chip for studying the impact of simulated microgravity as a novel pre-clinical approach in brain tumor therapy. *Adv Ther.* 2021;4:2100106. doi: 10.1002/adtp.202100106

18. Van Ombergen A, Chalupa-Gantner F, Chansoria P, et al. 3D bioprinting in microgravity: opportunities, challenges, and possible applications in space. *Adv Healthc Mater.* 2023;12:e2300443. doi: 10.1002/adhm.202300443

19. Kang HW, Lee SJ, Ko IK, et al. A 3D bioprinting system to produce human-scale tissue constructs with structural integrity. *Nat Biotechnol.* 2016;34:312-319. doi: 10.1038/nbt.3413

20. Mochi F, Scatena E, Rodriguez D, Ginebra M-P, Del Gaudio C. Scaffold-based bone tissue engineering in microgravity: potential, concerns and implications. *NPJ Microgravity.* 2022;8:45. doi: 10.1038/s41526-022-00236-1

21. Tu X, Delgado-Calle J, Condon KW, et al. Osteocytes mediate the anabolic actions of canonical Wnt/β-catenin signaling in bone. *Proc Natl Acad Sci USA.* 2015;112:E478-E486. doi: 10.1073/pnas.1409857112

22. Morey-Holton ER, Globus RK. Hindlimb unloading of growing rats: a model for predicting skeletal changes during space flight. *Bone.* 1998;22:83S-88S. doi: 10.1016/S8756-3282(98)00019-2

23. Wang P, Wang X, Wang B, Li X. 3D printing of osteocytic Dll4 integrated with PCL for cell fate determination towards osteoblasts in vitro. *Bio-Design Manuf.* 2022;5: 497-511. doi: 10.1007/s42242-022-00196-1

24. Gong W, Li M, Zhao L, et al. Sustained release of a highly specific GSK3β inhibitor SB216763 in the PCL scaffold creates an osteogenic niche for osteogenesis, anti-adipogenesis, and potential angiogenesis. *Front Bioeng Biotechnol.* 2023;11:1215233. doi: 10.3389/fbioe.2023.1215233

25. Liu Y, Ruan X, Li J, et al. The osteocyte stimulated by Wnt agonist SKL2001 is a safe osteogenic niche improving bioactivities in a polycaprolactone and cell integrated 3d module. *Cells.* 2022;11:831. doi: 10.3390/cells11050831

26. Yuste I, Luciano FC, González-Burgos E, Lalatsa A, Serrano DR. Mimicking bone microenvironment: 2D and 3D in vitro models of human osteoblasts. *Pharmacol Res.* 2021;169:105626. doi: 10.1016/j.phrs.2021.105626

27. Zhou Z, Pang Y, Ji J, et al. Harnessing 3D in vitro systems to model immune responses to solid tumours: a step towards improving and creating personalized immunotherapies. *Nat Rev Immunol.* 2024;24:18-32.

doi: 10.1038/s41577-023-00896-4

28. Hammond TG, Hammond JM. Optimized suspension culture: the rotating-wall vessel. *Am J Physiol Renal Physiol.* 2001;281:F12-F25.
doi: 10.1152/ajprenal.2001.281.1.F12

29. Wang X, Tu X, Ma Y, et al. Wnt3a-induced ST2 decellularized matrix ornamented PCL scaffold for bone tissue engineering. *Biocell.* 2022;46:2089-2099.
doi: 10.32604/biocell.2022.020069

30. Luo Y, Liu Y, Wang B, Tu X. CHIR99021-treated osteocytes with Wnt activation in 3D-printed module form an osteogenic microenvironment for enhanced osteogenesis and vasculogenesis. *Int J Mol Sci.* 2023;24:6008.
doi: 10.3390/ijms24066008

31. Zhang J, Zhang Y, Chen J, Gong W, Tu X. The osteocyte with SB216763-activated canonical Wnt signaling constructs a multifunctional 4D intelligent osteogenic module. *Biomolecules.* 2024;14:354.
doi: 10.3390/biom14030354

32. Liu G, Chen J, Wang X, Liu Y, Ma Y, Tu X. Functionalized 3D-printed ST2/gelatin methacryloyl/polcaprolactone scaffolds for enhancing bone regeneration with vascularization. *Int J Mol Sci.* 2022;23:8347.
doi: 10.3390/ijms23158347

33. Abraham RT. Identification of TOR signaling complexes: more TORC for the cell growth engine. *Cell.* 2002;111:9-12.
doi: 10.1016/s0092-8674(02)01009-7

34. Gschwendt M, Muller HJ, Kielbassa K, et al. Rottlerin, a novel protein kinase inhibitor. *Biochem Biophys Res Commun.* 1994;199:93-98.
doi: 10.1006/bbrc.1994.1199

35. Aderem A. The MARCKS brothers: a family of protein kinase C substrates. *Cell.* 1992;71:713-716.
doi: 10.1016/0092-8674(92)90546-o

36. Leupin O, Kramer I, Collette NM, et al. Control of the SOST bone enhancer by PTH using MEF2 transcription factors. *J Bone Miner Res.* 2007;22:1957-1967.
doi: 10.1359/jbmr.070804

37. Robling AG, Niziolek PJ, Baldridge LA, et al. Mechanical stimulation of bone in vivo reduces osteocyte expression of Sost/sclerostin. *J Biol Chem.* 2008;283:5866-5875.
doi: 10.1074/jbc.M705092200

38. Spatz JM, Fields EE, Yu EW, et al. Serum sclerostin increases in healthy adult men during bed rest. *J Clin Endocrinol Metab.* 2012;97:E1736-E1740.
doi: 10.1210/jc.2012-1579

39. Uda Y, Azab E, Sun N, Shi C, Pajevic PD. Osteocyte mechanobiology. *Curr Osteoporos Rep.* 2017;15:318-325.
doi: 10.1007/s11914-017-0373-0

40. Metzger CE, Anand Narayanan S, Phan PH, Bloomfield SA. Hindlimb unloading causes regional loading-dependent changes in osteocyte inflammatory cytokines that are modulated by exogenous irisin treatment. *NPJ Microgravity.* 2020;6:28.
doi: 10.1038/s41526-020-00118-4

41. Lau P, Vico L, Rittweger J. Dissociation of bone resorption and formation in spaceflight and simulated microgravity: potential role of myokines and osteokines? *Biomedicines.* 2022;10:342.
doi: 10.3390/biomedicines10020342.

42. Zhang Y, Zhao Y, Xie Z, Li M, Liu Y, Tu X. Activating Wnt/β-catenin signaling in osteocytes promotes osteogenic differentiation of BMSCs through BMP-7. *Int J Mol Sci.* 2022;23:16045.
doi: 10.3390/ijms232416045

43. Sapir-Koren R, Livshits G. Osteocyte control of bone remodeling: is sclerostin a key molecular coordinator of the balanced bone resorption-formation cycles? *Osteoporos Int.* 2014;25:2685-2700.
doi: 10.1007/s00198-014-2808-0

44. Yuan Z, Li Q, Luo S, et al. PPARγ and Wnt signaling in adipogenic and osteogenic differentiation of mesenchymal stem cells. *Curr Stem Cell Res Ther.* 2016;11:216-225.
doi: 10.2174/1574888x10666150519093429

45. Borner C, Guadagno SN, Fabbro D, et al. Expression of four protein kinase C isoforms in rat fibroblasts. Differential alterations in ras-, src-, and fos-transformed cells. *J Biol Chem.* 1992; 267:12900-12910.
doi: 10.1016/S0021-9258(18)42360-5

46. Ohno S, Akita Y, Hata A, et al. Structural and functional diversities of a family of signal transducing protein kinases, protein kinase C family; two distinct classes of PKC, conventional cPKC and novel nPKC. *Adv Enzyme Regul.* 1991;31:287-303.
doi: 10.1016/0065-2571(91)90018-h

47. Hug H, Sarre TF. Protein kinase C isoenzymes: divergence in signal transduction? *Biochem J.* 1993;291(Pt 2): 329-343.
doi: 10.1042/bj2910329

48. Fleming I, MacKenzie SJ, Vernon RG, et al. Protein kinase C isoforms play differential roles in the regulation of adipocyte differentiation. *Biochem J.* 1998;333(Pt 3):719-727.
doi: 10.1042/bj3330719

49. Tang Y, Wu X, Lei W, et al. TGF-beta1-induced migration of bone mesenchymal stem cells couples bone resorption with formation. *Nat Med.* 2009;15:757-765.
doi: 10.1038/nm.1979

50. Smith SM, Heer MA, Shackelford LC, et al. Benefits for bone from resistance exercise and nutrition in long-duration spaceflight: evidence from biochemistry and densitometry. *J Bone Miner Res.* 2012;27:1896-1906.
doi: 10.1002/jbmr.1647

51. Halloran BP, Bikle DD, Harris J, et al. Regional responsiveness of the tibia to intermittent administration of parathyroid

hormone as affected by skeletal unloading. *J Bone Miner Res.* 1997;12:1068-1074.
doi: 10.1359/jbmr.1997.12.7.1068

52. Spatz JM, Ellman R, Cloutier AM, et al. Sclerostin antibody inhibits skeletal deterioration in mice exposed to partial weight-bearing. *Life Sci Space Res (Amst).* 2017;12: 32-38.
doi: 10.1016/j.lssr.2017.01.001

53. Barbehenn EK, Lurie P, Wolfe SM. Osteosarcoma risk in rats using PTH 1-34. *Trends Endocrinol Metab.* 2001; 12:383.
doi: 10.1016/s1043-2760(01)00489-1

54. Hildreth BE, 3rd, Werbeck JL, Thudi NK, et al. PTHrP 1-141 and 1-86 increase in vitro bone formation. *J Surg Res.* 2010;162:e9-e17.
doi: 10.1016/j.jss.2010.02.023

55. Costa-Almeida R, Granja PL, Gomes ME. Gravity, tissue engineering, and the missing link. *Trends Biotechnol.* 2018;36:343-347.
doi: 10.1016/j.tibtech.2017.10.017

56. Artegiani B, Clevers H. Use and application of 3D-organoid technology. *Hum Mol Genet.* 2018;27:R99-R107.
doi: 10.1093/hmg/ddy187

57. He J, Zhang X, Xia X, et al. Organoid technology for tissue engineering. *J Mol Cell Biol.* 2020;12:569-579.
doi: 10.1093/jmcb/mjaa012

58. Yi SA, Zhang Y, Rathnam C, Pongkulapa T, Lee KB. Bioengineering approaches for the advanced organoid research. *Adv Mater.* 2021;33:e2007949.
doi: 10.1002/adma.202007949

59. Hwang YS, Cho J, Tay F, et al. The use of murine embryonic stem cells, alginate encapsulation, and rotary microgravity bioreactor in bone tissue engineering. *Biomaterials.* 2009;30:499-507.
doi: 10.1016/j.biomaterials.2008.07.028

60. Avitabile E, Fusco L, Minardi S, et al. Bioinspired scaffold action under the extreme physiological conditions of simulated space flights: osteogenesis enhancing under microgravity. *Front Bioeng Biotechnol.* 2020;8:722.
doi: 10.3389/fbioe.2020.00722

61. Hann SY, Cui H, Esworthy T, et al. Dual 3D printing for vascularized bone tissue regeneration. *Acta Biomater.* 2021;123:263-274.
doi: 10.1016/j.actbio.2021.01.012

62. Zhou F, Hong Y, Liang R, et al. Rapid printing of bio-inspired 3D tissue constructs for skin regeneration. *Biomaterials.* 2020;258:120287.
doi: 10.1016/j.biomaterials.2020.120287

63. Zhang W, Shi W, Wu S, et al. 3D printed composite scaffolds with dual small molecule delivery for mandibular bone regeneration. *Biofabrication.* 2020;12:035020.
doi: 10.1088/1758-5090/ab906e

64. Chen S, Shi Y, Zhang X, Ma J. Evaluation of BMP-2 and VEGF loaded 3D printed hydroxyapatite composite scaffolds with enhanced osteogenic capacity in vitro and in vivo. *Mater Sci Eng C Mater Biol Appl.* 2020;112:110893.
doi: 10.1016/j.msec.2020.110893

65. West-Livingston LN, Park J, Lee SJ, Atala A, Yoo JJ. The role of the microenvironment in controlling the fate of bioprinted stem cells. *Chem Rev.* 2020; 120:11056-11092.
doi: 10.1021/acs.chemrev.0c00126